Kinetics of Silicon Nitride Formation on SiO_2-Derived Rice Husk Ash Using the Chemical Vapor Infiltration Method

N. SOLTANI,[1,2] A. BAHRAMI,[1,2] M. I. PECH-CANUL,[1] L. A. GONZÁLEZ,[1] A. GURLO[3]

[1]*Centro de Investigación y de Estudios Avanzados del Instituto Politécnico Nacional, Cinvestav-Saltillo. Av. Industria Metalúrgica No. 1062 Parque Industrial Saltillo-Ramos Arizpe. Ramos Arizpe, 25900, Coahuila, México*

[2]*Instituto de Investigaciones en Materiales, Universidad Nacional Autónoma de México, Ciudad Universitaria, 04510, D.F., México*

[3]*Fachgebiet Keramische Werkstoffe/Chair of Advanced Ceramic Materials, Institut für Werkstoffwissenschaften und –technologien, Technische Universitaet Berlin, Hardenbergstraße 40, 10623, Berlin, Germany*

Received 28 September 2016; revised 29 November 2016; accepted 1 January 2017

DOI 10.1002/kin.21075
Published online 6 February 2017 in Wiley Online Library (wileyonlinelibrary.com).

ABSTRACT: Since silicon nitride coatings on silicon dioxide are attractive for the semiconductor and electronics industries, cognizance of their formation kinetics is crucial for optimization of production parameters. In this contribution, the deposition kinetics (rate constant and activation energy) of Si_3N_4 by the hybrid system chemical vapor infiltration route (HYSY-CVI), starting from N_2:NH_3 and SiF_4 (produced by the decomposition of Na_2SiF_6) has been studied. The deposition rate equation for Si_3N_4 was established from several possible gas-phase or surface reaction steps involved in the growth of Si_3N_4 coatings onto silica-derived rice husk ash (RHA). Based on a judicious analysis of four different models, it was found that Freundlich's adsorption model satisfactorily represents the rate of Si_3N_4 deposition process onto RHA. © 2017 Wiley Periodicals, Inc. Int J Chem Kinet 49: 293–302, 2017

INTRODUCTION

Si_3N_4 thin coatings prepared by chemical vapor deposition (CVD) are useful for realization of a large range of operations applied in the semiconductor technology, being utilized on a large scale for the fabrication and performance improvement of the electronic components. Since the Si_3N_4 coating properties depend to a considerable extent on the deposition conditions, the study of their formation kinetics is important for the optimization of the production parameters [1,2]. The commonly used approach for deriving a mechanism and kinetics of CVD is based on experimental results combined with reasonable assumptions.

Correspondence to: Niloofar Soltani; e-mail: niloofar.soltani@cinvestav.mx, nilufar.soltani@gmail.com.
© 2017 Wiley Periodicals, Inc.

Optimization of the coating deposition and properties often requires knowledge of gas-phase and surface reaction kinetics. The possible surface reactions, which can control the process rate for the simple deposition of a single element (and which are seen to be very temperature dependent), include (a) mass transport of reactant(s) to the substrate, (b) adsorption of reactant(s) onto the substrate surface, (c) chemical reaction on the surface (this could also include surface diffusion), and (d) desorption of product gas(es) from the surface. These reactions are collectively referred to as kinetic steps in the overall process [3]. It is widely recognized that both mass transport and surface reactions play the most important roles in the growth rate of the deposit. In chemical reaction limiting regime, the coatings of the CVD are relatively uniform since the supply of the reactant gaseous species to the substrate surface is sufficient for consumption through chemical reactions. Accordingly, this regime is usually operated by many CVD processes for coatings and an isothermal/isobaric CVI process for fiber-reinforced ceramic–matrix composites, whereas the mass transport rate can be enhanced considerably through a decrease in the total pressure. This is the main reason why most CVD processes are carried out at reduced pressures [3,4].

The deposition rate depends strongly on the substrate temperature, the gas flow rate, and the geometric orientation of the substrate in the reactor. A few kinetic models available in the literature for silicon nitride deposition are based on different assumptions about the mechanism of gas phase and surface reactions. One common way for depositing the coatings is the reaction of dichlorosilane (DCS, SiH_2Cl_2) with ammonia (NH_3). In the model suggested by Peev et al., a single power-law expression, rate $= k[SiH_2Cl_2]^{0.49}[NH_3]^{0.46}$ (Freundlich adsorption isotherm) has been used to fit to experimental data and no gas-phase reactions are considered [5]. Roenigk and Jensen have included gas-phase decomposition of DCS into dichlorosililene ($SiCl_2$) and hydrogen into their kinetic models [6]. The kinetic parameters of various silicon nitride coatings prepared by CVD were evaluated in silicon chloride, DCS, or silane with ammonia systems. It is reported that the rate constants for SiH_4 are higher than that obtained from SiH_2Cl_2 and $SiCl_4$ reaction [2]. In addition to these types of gases, system of solid silicon precursor (Na_2SiF_6) – precursor gaseous nitrogen (N_2, mixture N_2 and NH_3) has been employed in the synthesis of Si_3N_4 by HYSY-CVI (hybrid precursor system chemical vapor infiltration). Since this synthesis method combines the use of gas (N_2, NH_3, and N_2–NH_3 mix) and solid precursors (for instance, Na_2SiF_6), it is referred to as a hybrid precursor based method [7,8].

This route is a modified CVD process and hybrid system route developed in CINVESTAV–Saltillo campus. Thermal gradients of the reaction chamber are used for generating the silicon reactant gas (SiF_n) in situ by the thermal decomposition of sodium hexafluorosilicate (Na_2SiF_6) and to carry out the reaction between the gas precursor and nitrogen fed into the chamber to form Si_3N_4, which then may be deposited on porous or monolithic substrates [8,9].

The aim of this investigation is to study the deposition kinetics (rate constant and activation energy) of Si_3N_4, starting from N_2:NH_3 and SiF_4 produced from the decomposition of Na_2SiF_6. The equation of deposition rate of Si_3N_4 was established from several possible gas-phase or surface reaction steps involved in the coating growth of Si_3N_4 onto silica-derived rice husk ash (RHA). Although RHA and its ceramic derivative have been widely studied [10,11], to the authors' best knowledge, there is no study reported on the deposition of silicon nitride on its surface. Based on a careful analysis of four different models, a model is proposed and validated.

EXPERIMENTAL PROCEDURES

Rice husk was washed with distilled water to remove dirt and other contaminants and then was dried in open air for 1 day. The washed and dried rice husks were calcined at 950°C for 2 h in a muffle furnace and air atmosphere. Obtained RHA was ball milled for 10 min at the rotational speed of 120 rpm with alumina balls. Cylindrical preforms (1 cm diameter × 1.5 cm height) with 50% porosity were prepared by uniaxial compaction of SiO_2/Si (compaction pressure of 20 MPa) with 10 wt% Si. Likewise, cylindrical compacts (3 cm in diameter × 1 cm height) were prepared using an amount of 15 g of sodium hexafluorosilicate (Na_2SiF_6) using a compaction pressure of 25 MPa.

Processing of SiO_2/Si_3N_4 Composites via HYSY-CVI

The silica porous preforms were processed in a HYSY-CVI reactor, which consists of a horizontal tube furnace (3.175 cm diameter × 76 cm height) provided with end-cap fittings to control the process atmosphere, gas inlets (and outlets) to supply the nitrogen precursor, as well as devices to control gas flow rate and pressure. It also includes a powder collector and a neutralizer of the gas by-products (see Fig. 1). During tests, the silica preforms were consistently positioned in the center of the reaction chamber where a 10-cm length isothermal region is formed, and the Na_2SiF_6 compacts were

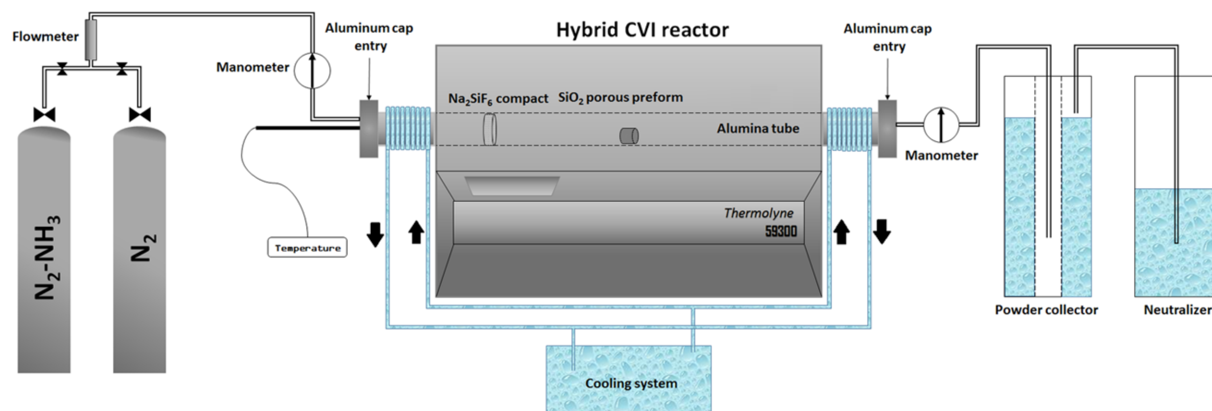

Figure 1 Schematic representation of the experimental setup. [Color figure can be viewed at wileyonlinelibrary.com]

placed nearby the gas entrance. More specifically, the Na_2SiF_6 (15 g) compacts were positioned within the alumina tube in a low-temperature zone between the gas entrance and the SiO_2/Si porous preforms. The strategic positioning of the Na_2SiF_6 compacts allows control on its decomposition rate in the temperature range of this study. The system was heated at a heating rate of 20°C min^{-1} in the N_{2-5} vol% NH_3 precursor up to the test temperature, held isothermally during 90 min test time and cooled down to room temperature in the same atmosphere. Chemical vapor infiltration trials were performed at a constant pressure, slightly above to that of the atmospheric pressure (gage pressure = 13 ± 1 mbar) in the reactor. An energy dispersive XRF spectrometer Bruker model S4 Pioneer with Rh X-ray was used to determine the chemical composition of rice husk and treated RHA. DTA/TG analyses were performed at atmospheric pressure in nitrogen on a SDT Q600 (V20.9 Build 20) equipment at heating rate of 20°C min^{-1}. To identify the phases formed, specimens were ground in a porcelain mortar up to mesh of 100 and then characterized by XRD using a diffractometer (Philips model 3040) under the following conditions: excitation voltage of the anode of 40 kV and current of 30 mA; monochromatic Cu $K\alpha$ radiation ($\lambda = 1.5418$ Å); 2θ range of 10–80°, at a scanning speed of 0.02° s^{-1}. The microstructure of the specimens was examined by a scanning electron microscope (Philips XL30 ESEM) provided with an EDX microanalysis device. Both, secondary and backscattered electron modes were used in the analyses, at an acceleration voltage between 20 and 30 kV. Raman spectra were obtained from the surface of the samples using a Horiba LABRAM 300 with a He-Ne Laser with 633 nm as the excitation source equipped with a cutoff filter and 100× magnification objective.

RESULTS AND DISCUSSION

Composition, Thermal Analysis, and Microstructure Characterization of RHA

The chemical compositions of rice husk and treated RHA are shown in Table I. As it can be observed from Table I, the calcination process increases the concentration of silica in the ash up to 96.45 wt%. The amounts of impurities are insignificant; thus their effects on the deposition process can be assumed negligible.

Figure 2 shows the TGA–DTA curves of the RHA. The TGA curve shows just one stage of weight loss (~1%) at stage A. At stage B (900–1300°C), one exothermic peak at 1205°C was observed, which is explained by the crystallization of amorphous SiO_2 into tridymite and cristobalite.

A representative X-ray diffraction pattern of silica produced from treated rice husk (RH) at 950ºC is shown in Fig. 3. Based on the treatment methods for

Table I Chemical Composition of Rice Husk and Treated RHA

Name	%Fe_2O_3	%Al_2O_3	%MgO	%K_2O	%P_2O_5	%CaO	%SiO_2	%LOI[a]
Rice husk	0.006	0.008	0.011	0.011	0.055	0.200	17.610	82.090
RHA	0.0359	0.078	0.297	0.321	0.0371	–	96.45	–

[a]LOI: Lost on ignition.

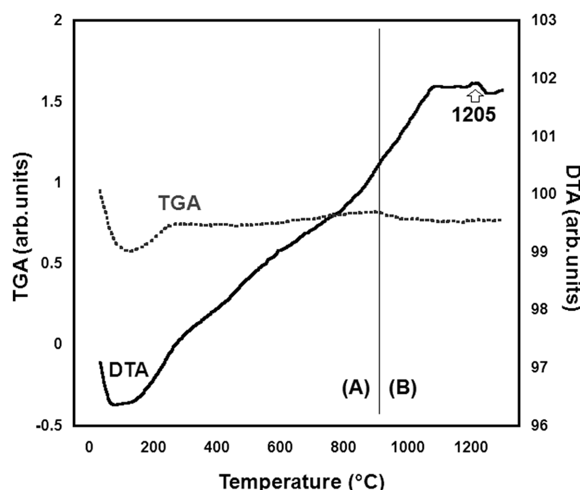

Figure 2 TGA and DTA thermograms of RHA.

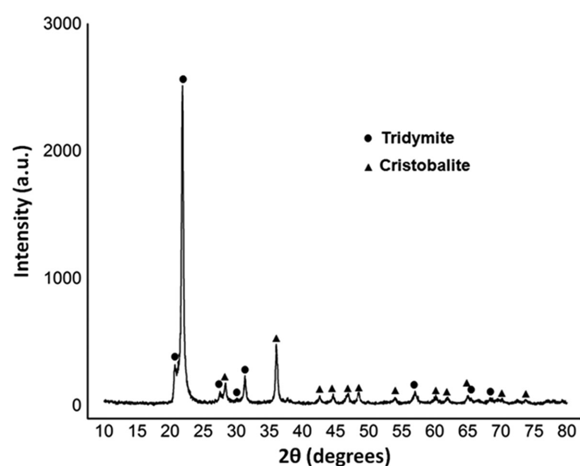

Figure 3 XRD pattern of silica produced from RH treated at 950ºC.

incineration of rice husk, amorphous or different types of crystalline silica can be obtained [12,13]. Using the aforementioned method of incineration, tridymite and cristobalite phases were detected in the XRD patterns.

Figure 4a shows the white and free-flowing nature of RHA. In Fig. 4b, the typical structural network of RHA is clearly observed. RHA shows a regular well-defined layered structure, appearing as a heterogeneous mass of coiled and fragmented sheets. The dome-shaped outline of the epidermal cells is responsible for the resemblance with "corn cob." A backbone structure shows that the organic molecules are arranged over the structural backbone in the natural state in a way similar to the bone and flesh arrangement in human beings.

Phase Analysis and Microstructure of Specimens Processed by HYSY-CVI

In Fig. 5, X-ray diffraction patterns from ground samples processed at 1200 and 1300°C for 90 min under NH_3:N_2 atmosphere with five gas flow rates are shown. As it can be seen from Fig. 5, in all the patterns the presence of Si, SiO_2, and Si_3N_4 was confirmed. The intensity of Si_3N_4 peaks is affected strongly by process temperature and gas flow rate. It is obvious from Figs. 5a and 5b that increasing temperature and gas flow rate cause intensification of deposited Si_3N_4 peaks.

The mole of Si_3N_4 was determined using the XPowder® computer software. By obtaining the weight percentage of each component, the mole fraction of Si_3N_4 was calculated. The results are shown in Table II. It can be seen that the mole percentage of Si_3N_4 increases with the increasing deposition temperature and N_2:NH_3 gas flow rate.

Figure 6 shows the Raman spectrum of the top side of deposited Si_3N_4 preform at 1300°C under various N_2:NH_3 flow rates at 90 min. A sharp peak at 515 cm^{-1} and relatively strong lines at 259, 365, 668, 868, 915, and 1034 cm^{-1} correspond to formation of α-Si_3N_4 [14]. It is clear the intensity of Si_3N_4 lines are highly dependent on the gas flow rate. At higher gas flow rate, the more intensified Si_3N_4 lines especially at 515 cm^{-1} can be observed.

Figure 7 shows scanning electron micrographs of the surface morphology of Si_3N_4 coatings deposited at various gas flow rates. As the gas flow rate increases from 20 to 100 cm^3 min^{-1}, the shape of the formed Si_3N_4 becomes more clearly defined. This is due to the fact that an increase in the gas flow rate, consequently, increases the concentration of reactants (higher supersaturation). At flow rates of 20 and 60 cm^3 min^{-1} due to low supersaturation, just the fine long fibers in their particular orientations can be observed; however, as the supersaturation is increased, the nucleation rate of other orientations becomes sufficiently greater than those under lower gas flow rates. Thus it can be concluded that fine fibers are formed at low levels of supersaturation, whereas dendrite shapes are favored at high supersaturation levels. As it can be seen from Fig. 7a, Si_3N_4 dendrites are distributed and grown evenly on RHA, whereas in Figs. 7b and 7c the free coated regions are observable.

As it can be seen in Fig. 8a, primary nuclei of Si_3N_4 are formed at $t = 45$ min. By increasing time up to 90 min, formation of Si_3N_4 nucleus is still observable while growth of short Si_3N_4 dendrites was already started. At 120 min, dramatic growth of Si_3N_4 fibers from the diameter of 520 nm at time of 90 min to the diameter of 950 nm was observed (Figs. 8b and 8c).

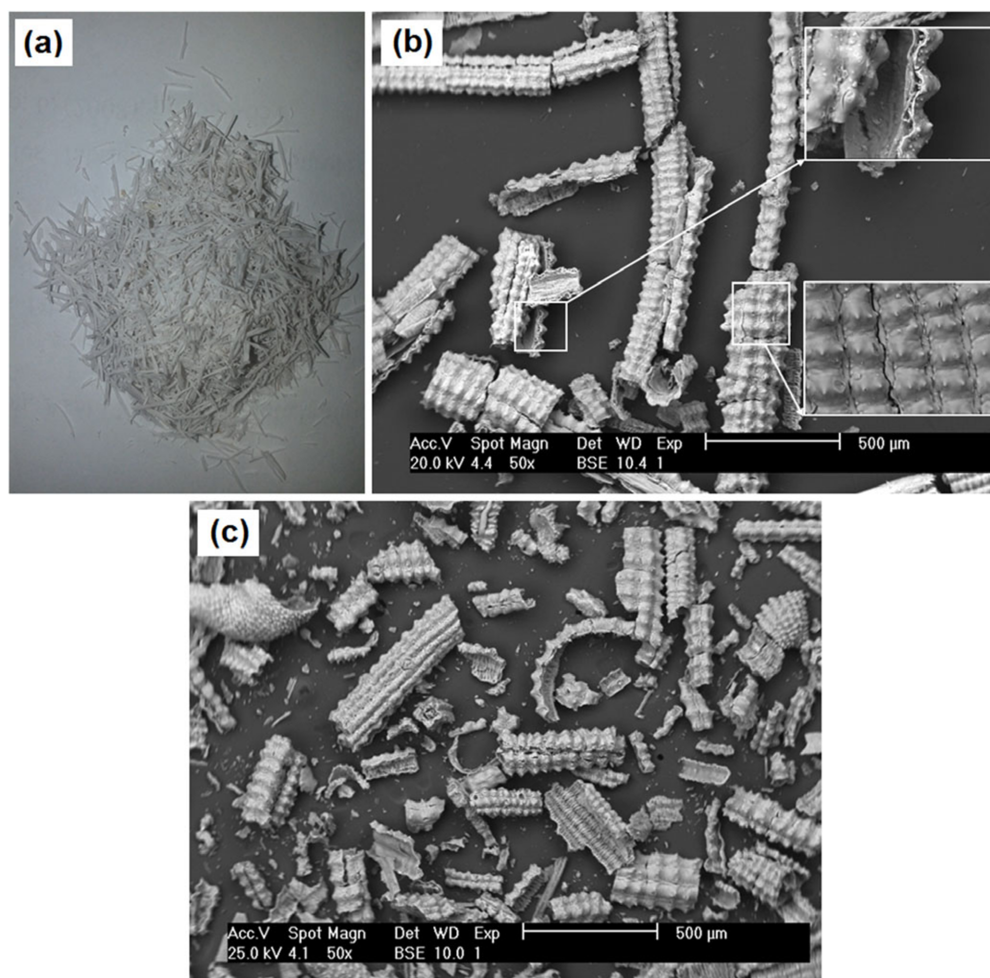

Figure 4 (a) White RHA obtained from incineration of treated RH, (b) SEM micrographs of RHA, and (c) ball-milled RHA. [Color figure can be viewed at wileyonlinelibrary.com]

In the following sections, a kinetic study of deposition of Si_3N_4 onto SiO_2-derives RHA is discussed.

Analysis of the Growth Kinetics of Si_3N_4

To predict silicon nitride growth rates from the modeling equations, kinetics of the various gas-phase and surface reaction steps must be specified. The model is simplified as follows:

1. Surface kinetics controls the system. It has been possible in this manner to evenly coat the internal surfaces of a porous body [15].
2. Formation of silicon–nitrogen bonds in gas-phase mixtures of SiF_4, nitrogen and ammonia accompanied by H_2 or F_2 elimination.
3. Formation of silicon–nitrogen bonds via one step without decomposition of SiF_4, N_2, and NH_3 on the substrate surface. The natural bond dissociation energies for $SiF_4 \rightarrow SiF_3 + F$, $NH_3 \rightarrow NH_2 + H$, and $N_2 \rightarrow 2N$ are 6.94, 10.2, and 15.57 eV, respectively.

The equations describing the deposition rate of Si_3N_4 can be based on the following models, summarized in Table III.

Using the data condensed in Table II, the rate of chemical reaction process was calculated by means of Eq. (1):

$$J = \frac{1}{S}\frac{\mathrm{d}N}{\mathrm{d}t} = \frac{R_D \rho_{\mathrm{Si_3N_4}}}{M_{\mathrm{Si_3N_4}}} \tag{1}$$

where J is the rate of chemical reaction (mol cm^{-2} s^{-1}), ρ is film density (g cm^{-3}), S is area (cm^2), R_D is the growth rate of the film (cm s^{-1}), M is molecular mass

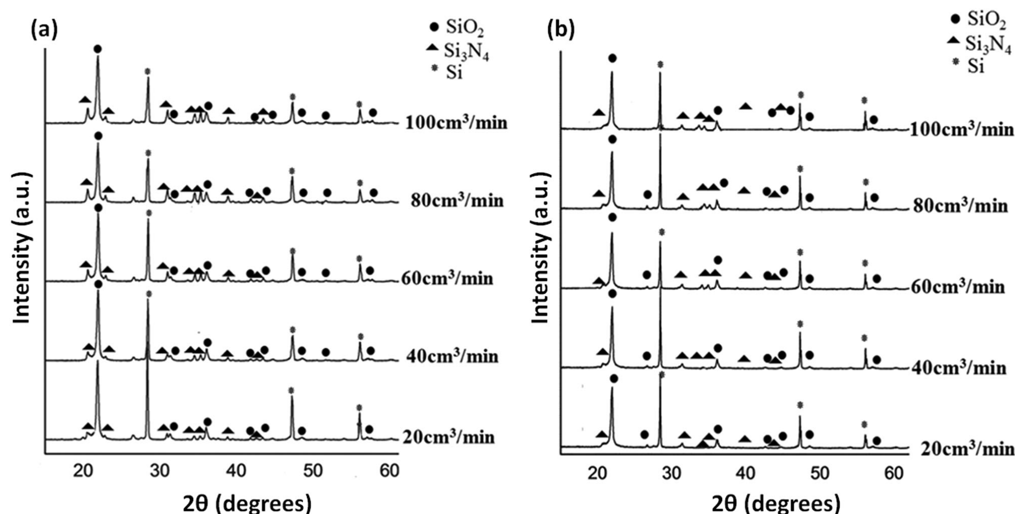

Figure 5 XRD patterns of Si_3N_4 deposited onto preforms under various gas flow rates for 90 min at (a) $T = 1300$ºC and (b) $T = 1200$ºC.

Table II Amount of Deposited Si_3N_4 (mol)

Temperature (ºC)	Gas Flow Rate (cm^3 min^{-1})				
	20	40	60	80	100
1300	0.0235	0.06804	0.123	0.158	0.238
1200	0.0118	0.023	0.033	0.041	0.0596

(g mol^{-1}), and t is the duration of the deposition process(s).

Assessment of the Preform Area. Since our modeling approach is based on the surface reactions, it is necessary to evaluate the contact area between RHA and the gas phase to estimate the total number of "surface sites." All experimental tests presented in this work were made with silica with an initial mass of 1 g. The shape of the RHA can be considered as a rectangular solid with domes on the top of its surface as shown in Fig. 4b. If we neglect the contact area between the domed plate shapes, then the preform can be seen as a single domed rectangular solid with a width of w and a length L. The relation between the density mass of the rice husk and its "hypothetical" length is

$$\rho = \frac{m_{\text{fiber}}}{\left(wtl + N\left(\frac{2\pi r^3}{3}\right)\right)} \tag{2}$$

where ρ is the density of RHA 1.6 (g cm^3), m is mass of the RHA 1 (g), r is the radius of dome 2.5×10^{-3} (cm), l is a hypothetical length of rice husk (cm),

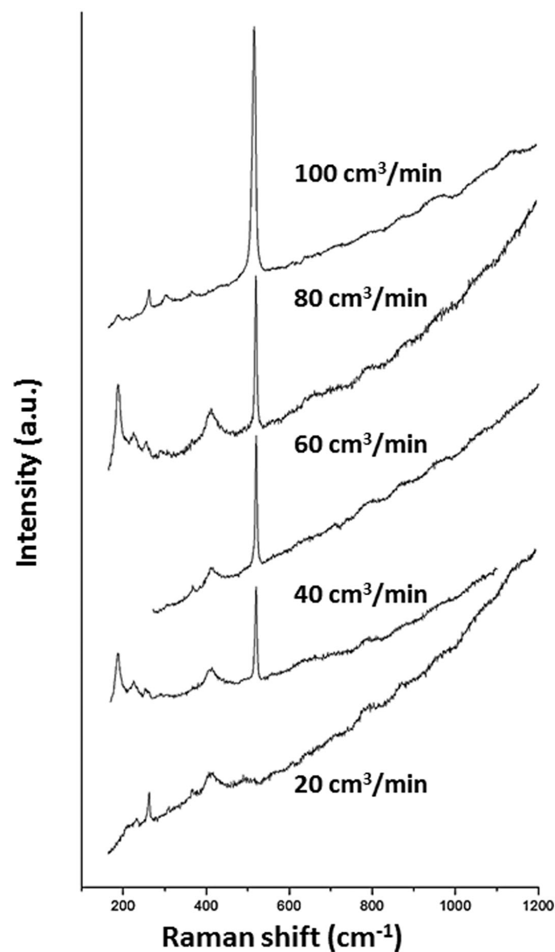

Figure 6 Raman spectra of α-Si_3N_4 taken from a top surface of samples: $T = 1300$ ºC under various N_2:NH_3 flow rates for 90 min.

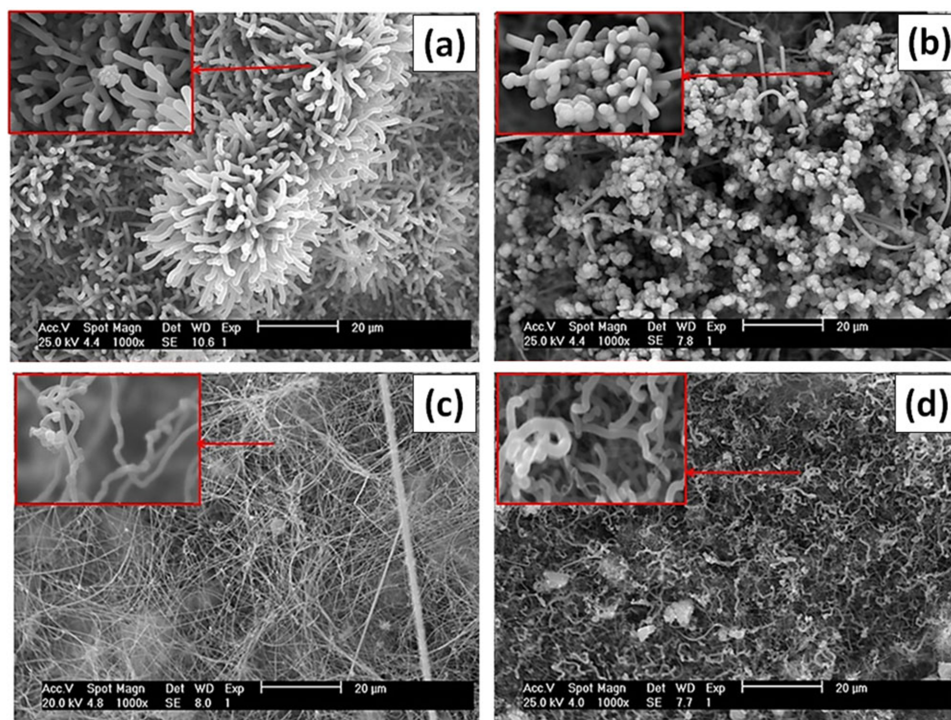

Figure 7 SEM photomicrographs showing Si_3N_4 deposited at 1300ºC for 90 min under gas flow rates of N_2:NH_3: (a) 100, (b) 80, (c), 60, and (d) 20 cm^3 min^{-1}. [Color figure can be viewed at wileyonlinelibrary.com]

t is the thickness of the RHA: 10^{-3} (cm), w is the width of the RHA: 0.04 (cm), n is the number of domes: in 2 $\times$ 10^{-4} (cm^2) it is equal to 8, and N is theTotal number of domes; $N = 8(l/2r)$.

Using Eq. (2), the length of the RHA can be estimated at 10,800 (cm). The contact area between the RHA and gas phase can then be estimated with Eq. (3):

$$S = 2lw + N\pi r^2 \tag{3}$$

By using Eq. (3), $S = 1212$ cm^2 for a preform that has an initial mass of 1 g was obtained.

A schematic of the surface site of deposition of Si_3N_4 based on the SEM observation is shown in Fig. 9.

Components in the Reactive Gas Mix. The molar concentration of $SiF_{4\,(g)}$ is determined based on the weight loss of the Na_2SiF_6 compacts during the tests. At constant temperature (580°C), the gas flow rate influences the decomposition of Na_2SiF_6. Under gas flow rate of 20, 40, 60, 80, and 100 cm^3 min^{-1}, the mole production of SiF_4 are 2.7 $\times$ 10^{-4}, 4.02 $\times$ 10^{-4}, 5.2 $\times$ 10^{-4}, 5.62 $\times$ 10^{-4}, and 6.1 $\times$ 10^{-4}, respectively. Decomposition kinetics of Na_2SiF_6 to SiF_4 under different N_2-NH_3 was discussed in details elsewhere [9].

The reaction at the Na_2SiF_6 surface is given by

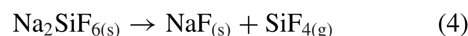

$$Na_2SiF_{6(s)} \rightarrow NaF_{(s)} + SiF_{4(g)} \tag{4}$$

Table IV shows the concentration of the gas components in the reactant mix, indicating how variations in the feeding flow rate lead to changes in gas concentration.

Validation of Models. To confirm the validity of the models, the rate of chemical reaction (J) values, calculated from Eq. (5) at $T = 1300$ºC and various molar concentrations of the reactants were substituted into the proposed modeling equations (Table III formula 1–4.2). The rate of chemical reaction was obtained for each gas flow rate by having values of mole fraction of Si_3N_4 taken from Table II. To determine the coefficients a, b, c, d, e, f, and g in Eqs. (1), (2), (3), (4.1), and (4.2) presented in Table III, an attempt to solve the equations was made. However, Eqs. (1), (3), (4.1), and (4.2) in Table III could not be resolved because the coefficients values are negative and infinite, having no real and physical meaning. Therefore, those models were discarded. Just Eq. (2), based on Freundlich's adsorption isotherm was resolved satisfactorily. Freundlich's isotherm is based on the assumption

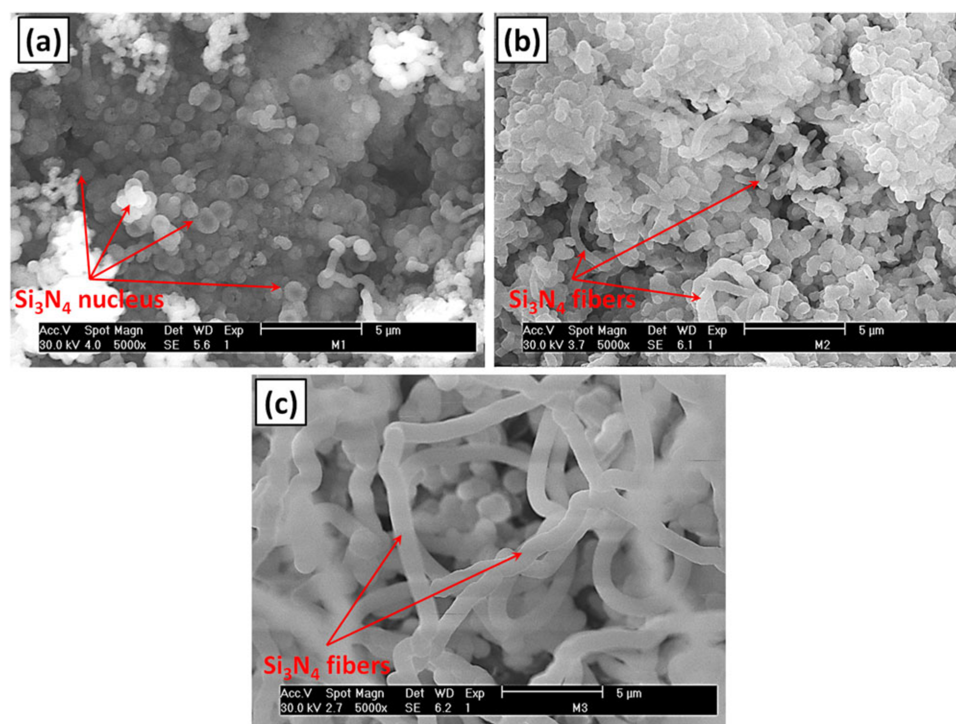

Figure 8 SEM photomicrographs showing Si_3N_4 deposited at 1300 ºC in N_2:NH_3 under the flow rate of 100 cm^3 min^{-1} for (a) 45 min, (b) 90 min, and (c) 120 min. [Color figure can be viewed at wileyonlinelibrary.com]

Table III Selected Modeling Equations to Predict Silicon Nitride Growth Rates

No.	Kinetic Models	Mathematical Model
1	Langmuir–Hinshelood	$\left(\frac{C_{N_2}C_{NH_3}C_{SiF_4}}{J}\right)^{\frac{1}{3}} = a + bC_{SiF_4} + cC_{NH_3} + dC_{N_2}$
2	Freundlich isotherm	$\log J = a + b\log C_{SiF_4} + c\log C_{NH_3} + d\log C_{N_2}$
3	Langmuir's adsorption isotherm	$\frac{C_{SiF_4}C_{NH_3}C_{N_2}}{J} = 1 + aC_{SiF_4} + bC_{NH_3} + cC_{N_2} + dC_{SiF_4}C_{NH_3} + eC_{SiF_4}C_{N_2} + fC_{NH_3}C_{N_2}$
4.1	Langmuir–Rideal or Eley–Rideal mechanism	$\left(\frac{C_{N_2}C_{NH_3}C_{SiF_4}}{J}\right)^{\frac{1}{2}} = a + bC_{SiF_4} + cC_{NH_3} + dC_{N_2}$
4.2		$\frac{C_{N_2}C_{NH_3}C_{SiF_4}}{J} = a + bC_{SiF_4} + cC_{NH_3} + dC_{N_2}$

that adsorption is nonuniform with some sites having higher adsorption coefficients and so being covered by molecules first. These sites have a more exothermic heat of adsorption. The surface concentrations of the reactants in this case will be power functions of their concentrations in the gas mixture [5]. Coefficients of Freundlich's isotherm *a*, *b*, *c*, and *d* were calculated 3.42, 0.71, 1.03, and 0.015, respectively. According to the obtained results, due to possessing of higher power, SiF_4 and NH_3 are the most satisfactory reactants. The calculated data show that increasing the NH_3/SiF_4 from 0.16 to 0.36 causes an increment of the deposition rate. Lee et al. showed that increasing the NH_3/SiF_4 to 3 increased the deposition rate [16]. However, by increasing NH_3 in the reactants, HF as a by-product of the CVI process increases subsequently. HF does not dissociate on Si_3N_4 and therefore causes an etch-like mark on Si_3N_4, and this etching causes an undesired loss of material; hence for avoiding the etching, the low ratio of NH_3/SiF_4 has been chosen in our study [17].

Calculation of Activation Energy. The activation energy E_a can be calculated from a plot of the logarithm of the growth rate as a function of deposition temperature. To describe the temperature relationship of

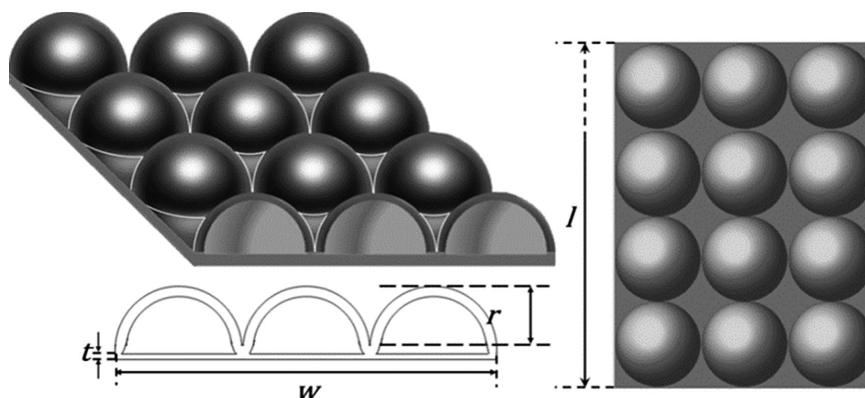

Figure 9 Schematic of the surface site of deposition of Si_3N_4.

Table IV Concentration of the Components in the Reactive Gas Mix

Gas Flow Rate (cm^3 min^{-1})	C_{N_2} ($mol\,cm^{-3}$)	C_{NH_3} ($mol\,cm^{-3}$)	C_{SiF_4} ($mol\,cm^{-3}$)
20	1.58×10^{-6}	8.31×10^{-8}	5.04×10^{-7}
40	3.16×10^{-6}	1.66×10^{-7}	7.5×10^{-7}
60	4.74×10^{-6}	2.49×10^{-7}	9.7×10^{-7}
80	6.31×10^{-6}	3.32×10^{-7}	1.05×10^{-6}
100	7.92×10^{-6}	4.16×10^{-7}	1.14×10^{-6}

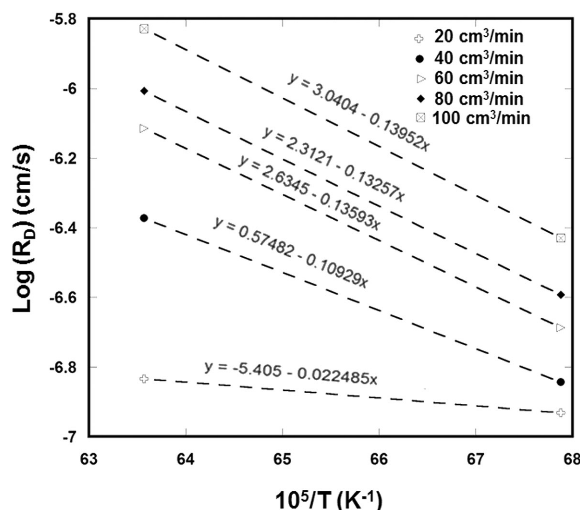

Figure 10 Temperature dependence of the growth rate.

the apparent rate constant, the following equation is recommended [5]:

$$K = A \exp\left(-\frac{E_a}{RT}\right) \tag{5}$$

where K is an apparent rate constant, A is a preexponential factor, E_a is activation energy of the process (J mol^{-1}), R is the gas constant 8.34 J mol^{-1} K^{-1}, and T is the deposition temperature (K). The range value of the activation energy in the deposition temperature range (1200–1300°C) is 110 kJ mol^{-1}, which is within the chemical reaction regime. However, de la Peña and Pech-Canul showed that the activation energy for Si_3N_4 formation into silicon porous preform under N_2–5% NH_3 is 48.3 kJ mol^{-1} [18]. This suggests that the adsorption affinity of silicon for reactive gases is much stronger than that for silica, making silicon a surface with energetic heterogeneities with reactive sites that greatly aid the adsorption.

By substitution of the coefficients of a, b, c, and d calculated in the preceding section and the value of activation energy into Freundlich's isotherm, the growth rate of deposited Si_3N_4 at 1300°C, can be calculated by

$$J = 1.5 \times 10^4 \exp(-13200/T)\, C_{SiF_4}^{0.71} C_{N_2}^{0.015} C_{NH_3}^{1.03} \tag{6}$$

As it can be seen in Fig. 10, the deposition rate increases with an increase in temperature and the growth rate gradually increases with increasing the gas flow rate, until the value of growth rate gets closer for higher gas flow rates. The variation of the growth rate confirms that the process is controlled kinetically. Increasing the deposition rate by temperature from 1200 to 1300 ºC indicates that the rate-limiting mechanism is surface chemical kinetics, i.e. chemisorption, and/or chemical reaction, surface migration, lattice incorporation and

desorption. These surface processes strongly depend on the deposition temperature [19].

CONCLUSIONS

In this work, the deposition kinetics (rate constant and activation energy) of Si_3N_4, starting from N_2:NH_3 and SiF_4 produced by the decomposition of Na_2SiF_6 has been studied. Key processing parameters, which govern deposition kinetics and its effects on the Si_3N_4 deposition were identified. It was found that deposition temperature is the parameter that most significantly influences the deposition rate and that gas flow rate affects coating uniformity and deposit morphology. The kinetics data obtained in this investigation provide the basis for analysis and developing a mathematical model aimed at elucidating the governing mechanisms of the HYSYCVI-Si_3N_4 process. The process of silicon nitride coating growth at atmospheric pressure is described by a power-law kinetics equation derived from the prerequisite that the interaction proceeds between reactant molecules adsorbed on an energetically heterogeneous surface. Increasing the deposition rate by temperature increment from 1200 to 1300ºC indicates that the rate-limiting step is surface chemical reaction. Based on an analysis of four different models, it was found that Freundlich's adsorption model satisfactorily represents the rate of Si_3N_4 deposition process onto RHA.

Ms. Niloofar Soltani and Mr. Amin Bahrami gratefully acknowledge CONACyT (Consejo Nacional de Ciencia y Tecnología, en México) for granting a doctoral scholarship. The authors also acknowledge Dr. Drik Heinrich and Dr. Ulla Simon from Technische Universität, Berlin, Germany, for Raman spectroscopy analyses and Dr. Jose Cruz Flores Garcia, Mr. Sergio Rodríguez-Arias, and Mr. Felipe Marquez-Torres from CINVESTAV-IPN, Mexico, for their technical assistance during, experimental procedure, XRD and SEM, respectively.

BIBLIOGRAPHY

1. Soltani, N.; Bahrami, A.; Pech-Canul, M. I.; González, L. A. Chem Eng J 2015, 264, 899–935.
2. Morosanu, C.; Segal, E. Mater Chem 1982, 7, 79–87.
3. Bryant, W. J Mater Sci 1977, 12, 1285–1306.
4. Xu, Y.; Yan, X.-T. Chemical Vapour Deposition: An Integrated Engineering Design for Advanced Materials; Springer, London, 2010, 129–164.
5. Peev, G.; Zambov, L.; Yanakiev, Y. Thin Solid Films 1990, 189, 275–282.
6. Roenigk, K. F.; Jensen, K. F. J Electrochem Soc 1987, 134, 1777–1785.
7. Flores-García, J.; Pech-Canul, M. I.; Leal-Cruz, A.; Rendón-Angeles, J. J Eur Ceram Soc 2012, 32, 175–184.
8. Leal-Cruz, A.; Pech-Canul, M.; Lara-Curzio, E.; Trejo, R.; Peascoe, R. Mater Chem Phys 2009, 114, 376–381.
9. Soltani, N.; Pech-Canul, M. I.; González, L. A.; Bahrami, A. Int J Chem Kinet 2016, 48, 379–395.
10. Bahrami, A.; Soltani, N.; Pech-Canul, M. I.; Gutiérrez, C. A. Crit Rev Environ Sci Technol 2015, 1–66.
11. Bahrami, A.; Simon, U.; Soltani, N.; Zavareh, S.; Schmidt, J.; Pech-Canul, M. I.; Gurlo, A. Green Chem 2017, 19(1), 188–195.
12. Bahrami, A.; Pech-Canul, M. I.; Gutierrez, C. A.; Soltani, N. J Alloys Compd 2015, 644, 256–266.
13. Bahrami, A.; Pech-Canul, M. I.; Gutiérrez, C. A.; Soltani, N. Appl Surf Sci 2015, 357(part A), 1104–1113.
14. Kuzuba, T.; Kijima, K.; Bando, Y. J Chem Phys 1978, 69, 40–42.
15. Bryant, W. A. J Mater Sci 1977, 12, 1285–1306.
16. Lee, W. Y.; Strife, J. R.; Veltri, R. D. J Am Ceram Soc 1992, 75, 2200–2206.
17. Outka, D. A. MRS Proc. 1991, p 79.
18. De la Pena, J.; Pech-Canul, M. I. Ceram Int 2007, 33, 1349–1356.
19. Choy, K.; Derby, B. J Phys II 1991, 1, 697.